IL NUOVO CIMENTO Vol. 35 C, N. 6 Novembre-Dicembre 2012
DOI 10.1393/ncc/i2012-11367-5

Colloquia: LaThuile12

Latest B physics results from ATLAS

J. Kirk on behalf of the ATLAS Collaboration
Rutherford Appleton Laboratory - Chilton, Oxfordshire, UK

ricevuto il 7 Settembre 2012

Summary. — B physics results from the ATLAS detector at the LHC are presented using data collected during 2010 and 2011. Inclusive production cross-sections for quarkonia are measured and compared to theoretical predictions. Both the average B-hadron lifetime and the lifetime of exclusively reconstructed B_d^0 and B_s^0 mesons are presented. A first observation of the $\chi_b(3P)$ $b\bar{b}$ state is also reported.

PACS 13.20.Gd – Decays of J/Ψ, Υ, and other quarkonia.
PACS 14.40.Nd – Bottom mesons ($|B| > 0$).
PACS 14.40.Pq – Heavy quarkonia.

1. – Introduction

The ATLAS detector [1] at the Large Hadron Collider (LHC) is designed as a general-purpose detector with the main focus on high-momentum discovery physics. However, it also has a dedicated B physics programme, the latest results from which are presented here. The B physics programme concentrates on low momentum dimuon B signatures which can be efficiently triggered at an affordable event rate. This allows the study of quarkonia production (an important test of QCD), B-hadrons decaying to $J/\psi X$ (for mixing and CP violation studies) and the search for rare decays of B-hadrons into final states containing two muons.

The most important elements of the detector for B physics measurements are the Inner Detector tracker and the Muon Spectrometer. The Inner Detector consists of silicon pixel and microstrip detectors and a transition radiation tracker covering $|\eta| < 2.5$ and immersed in a 2 T magnetic field. The Muon Spectrometer covers $|\eta| < 2.7$, it consists of precision tracking chambers and detectors designed for triggering, both of which are within a toroidal magnetic field of 0.5 T. During 2010 and 2011 ATLAS has recorded 48 pb^{-1} and 5.6 fb^{-1} of data from p-p collisions at a centre-of-mass energy $\sqrt{s} = 7$ TeV.

During low luminosity data-taking in early 2010 B physics events could be triggered using low momentum single muons. With increasing luminosity these triggers were either prescaled or had increased thresholds applied which severely limits the acceptance for B physics events. For this reason, dedicated B physics triggers based on dimuons had been

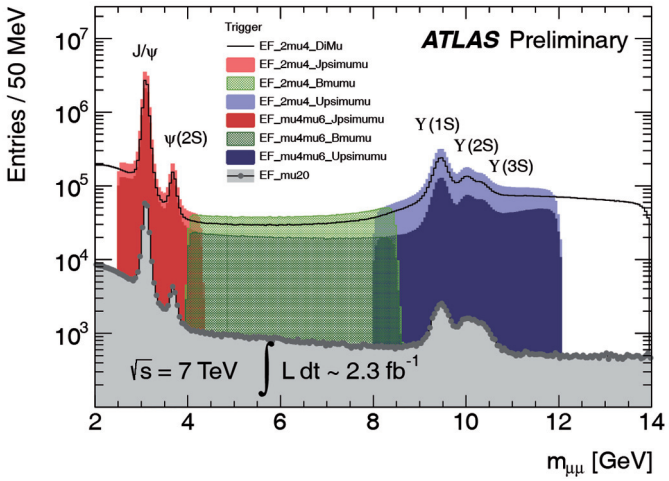

Fig. 1. – Invariant mass of oppositely charged muon candidate pairs selected by a variety of ATLAS triggers. The coloured histograms show those events selected by the dedicated Bphysics triggers compared to those triggered by the single muon trigger (grey). The different colours correspond to triggers with different mass ranges (red: 2.5–4.3 GeV ("Jpsimumu"), green: 4–8.5 GeV ("Bmumu"), blue: 8–12 GeV ("Upsimumu")).

developed. These require two low-momentum muons ($p_T > 4\,\text{GeV}$) to be identified at the first (hardware) level of the trigger. Once the muons are confirmed in the High Level Trigger, a fit is performed to the combined vertex and mass constraints are applied.

Figure 1 shows the dimuon mass spectrum for events recorded during the first half of 2011 data taking. It was possible to run the lowest theshold ("2mu4") triggers unprescaled for the whole of the 2011 data-taking period. The coloured histograms show the significant data sample collected by the dedicated B physics triggers.

2. – Quarkonia production measurements

Quarkonia (J/ψ and Υ) production has been studied since the discovery of the particles in the 1970s but it is still not fully understood. In particular, there is no explanation of the production mechanism which can explain both cross-section and spin-alignment measurements from previous experiments. The LHC provides the opportunity to test existing models at a higher energy regime, higher transverse momentum scale and wider rapidity range than previously.

Using $2.2\,\text{pb}^{-1}$ of data from 2010, ATLAS has measured the inclusive $J/\psi \to \mu^+\mu^-$ cross-section and the fraction of J/ψ which are produced non-promptly via decay of a B-hadron [2]. By combining these two measurements, separate cross-sections for the prompt and non-prompt J/ψ are also made.

The selected J/ψ events are corrected event-by-event for detector acceptance, reconstruction efficiency and trigger efficiency. An unbinned maximum-likelihood fit to the J/ψ mass spectrum is used to extract the cross-section in bins of rapidity and transverse momentum (p_T). Figure 2 shows the inclusive J/ψ cross-section for one rapidity bin. The largest source of systematic uncertainty on the measurement of the J/ψ cross-section is due to the spin alignment of the J/ψ which is unknown and affects the kinematic acceptance. Five extreme spin alignment scenarios are considered and maximum devia-

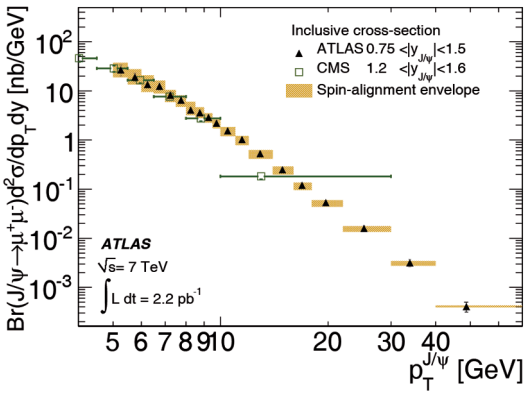

Fig. 2. – Inclusive J/ψ cross-section as a function of J/ψ transverse momentum for the rapidity bin $0.75 < |y| < 1.5$. The equivalent results from CMS are overlaid. The luminosity uncertainty (3.4%) is not shown.

tions of the acceptance correction are assigned as systematic effects. These uncertainties are regarded as theoretical rather than experimental and are shown in fig. 2.

At the LHC, J/ψ can be produced either promptly from the hard interaction or non-promptly via the decay of a B-hadron. It is possible to distinguish the J/ψ from b-decays from those produced promptly as the prompt decays occur at the primary vertex while the non-prompt J/ψ have a measurably displaced dimuon vertex due to the long lifetime of the parent B-hadron. The pseudo-proper time (τ) (using the mass and transverse momentum of the J/ψ rather than those of the B-hadron) is used as a discriminant:

$$\tau = \frac{L_{xy}\ m_{\mathrm{PDG}}^{J/\psi}}{p_T^{J/\psi}}\,. \tag{1}$$

where L_{xy} is the transverse decay length of the J/ψ vertex. The sample is divided into bins of p_T and rapidity of the J/ψ candidates. In each bin, a simultaneous unbinned maximum likelihood fit to the invariant mass and pseudo-proper time is performed to extract the fraction of J/ψ produced via B-decays. Figure 3 shows the pseudo-proper time distribution (left) and the non-prompt fraction (right) for one bin and the fraction results are compared to those from CDF and CMS. The non-prompt fraction increases rapidly with p_T and no significant rapidity dependence is observed. The results agree well with both the CMS and CDF results where they overlap. The agreement with CDF indicates that there is no dependence of the fraction on the collision energy.

By combining the information from the inclusive cross-section and the non-prompt B-fraction (F) it is possible to extract the non-prompt and prompt cross-sections separately; the prompt cross-section can be derived by multiplying the inclusive production cross-section by $(1 - F)$. Figure 4 shows the non-prompt (left) and prompt (right) J/ψ production cross-sections as a function of J/ψ transverse momentum compared to theoretical predictions. The measured non-prompt cross-section is in good agreement with Fixed-Order Next-to-Leading-Log theoretical predictions [3]. The prompt cross-section is compared to colour singlet (CSM) NLO and NNLO* pQCD predictions [4] and to the phenomenological Colour Evaporation Model (CEM) [5]. The CEM prediction is generally lower than the data and does not describe the shape of the distribution well. The

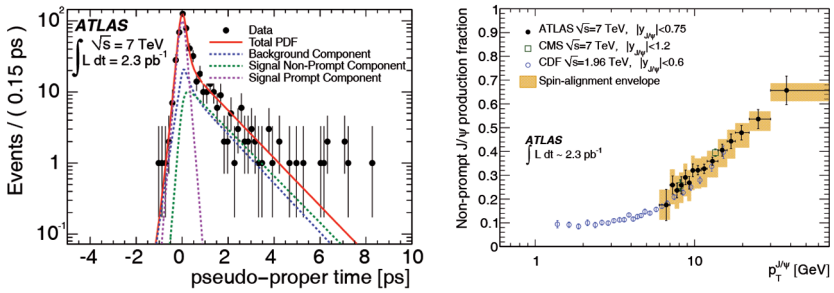

Fig. 3. – Left: Pseudo-proper time distribution of $J/\psi \to \mu^+\mu^-$ candidates for a selected p_T bin ($9.5 < p_T < 10.0\,\text{GeV}$) in the $|y| < 0.75$ rapidity bin. The points are data, the solid line is the result of the unbinned maximum-likelihood fit. Right: J/ψ non-prompt fraction as a function of J/ψ transverse momentum. Overlaid is a band representing the variation of the result under various spin-alignment scenarios. Results from CMS and CDF are also shown.

CSM predictions describe the shape better and the NNLO* prediction shows a significant improvement in the normalisation over the NLO prediction.

Using $1.1\,\text{pb}^{-1}$ of 2010 data, an unbinned maximum-likelihood fit to the $\Upsilon(1S)$ invariant mass spectrum is used to measure the cross-section in bins of rapidity and transverse momentum [6]. In this case the measurement is restricted to the fiducial region $p_T^\mu > 4\,\text{GeV}$, $|\eta^\mu| < 2.5$ to remove the spin alignment uncertainty. An example of the unfolded differential cross-section in one rapidity bin is shown in fig. 5. The data are compared to the colour singlet NLO (CSM) prediction and significant disagreement is observed. However, the prediction does not include feed-down from higher mass states which was estimated to contribute a factor of two at the Tevatron. A comparison is also made to predictions from PYTHIA 8.135 using NRQCD, the shape of the data distribution is not well described although the overall nomalisation agrees within a factor 2.

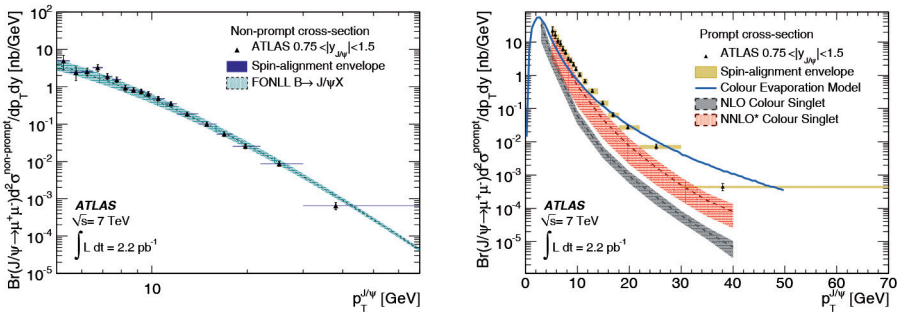

Fig. 4. – Non-prompt (left) and prompt (right) J/ψ production cross-sections as a function of J/ψ p_T. The non-prompt cross-section is compared to predictions from FONLL theory. The prompt cross-section is compared to predictions from NLO and NNLO* calculations, and the Colour Evaporation Model. Overlaid are bands representing the variation of the result under various spin-alignment scenarios representing a theoretical uncertainty on the non-prompt and prompt component.

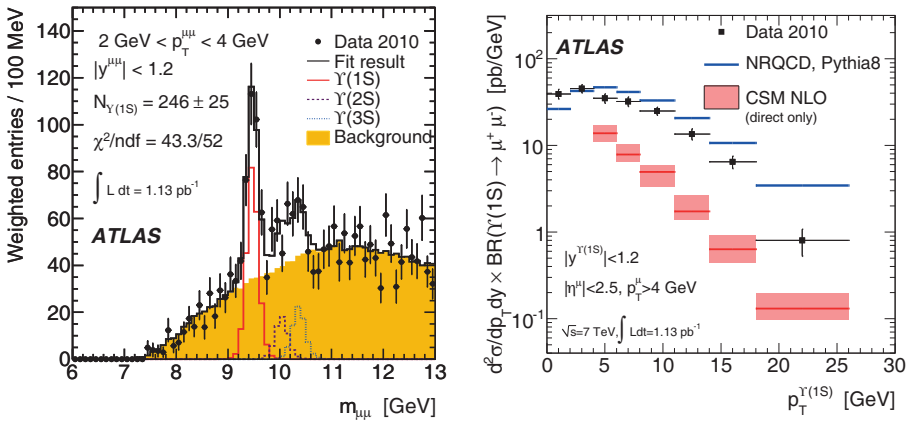

Fig. 5. – Left: Dimuon mass distribution for a representative bin in rapidity and p_T. The data (filled circles) are shown together with the result of the unbinned maximum-likelihood fit (histogram). Right: $\Upsilon(1S)$ cross-section for the $|y^{\Upsilon(1S)}| < 1.2$ rapidity bin as a function of $p_T^{\Upsilon(1S)}$, for $p_T^{\mu} > 4\,\text{GeV}$ and $|\eta^{\mu}| < 2.5$ on both muons. Also shown is the CSM prediction and the NRQCD prediction as implemented in PYTHIA8 for a particular choice of parameters.

3. – B-hadron properties

In ATLAS, B-hadrons can be reconstructed exclusively from their decays to J/ψ, *i.e.* $B \to J/\psi(\mu^+\mu^-)X$. A number of B-hadrons have been observed in ATLAS through such decays [7]. Some of these are useful as reference channels for other measurements, *e.g.* $B^{\pm} \to J/\psi K^{\pm}$ is used as a reference in the search for the rare B-decay $B_s \to \mu^+\mu^-$. Other channels will be used in the future for important physics measurements, *e.g.* $B_s^0 \to J/\psi\phi$ for CP violation studies, $\Lambda_b \to J/\psi\Lambda$ for the measurement of the Λ_b polarisation. Two example invariant mass distributions are shown in fig. 6 for $\Lambda_b \to J/\psi\Lambda(p^+\pi^-)$ (left) and $B_d^0 \to J/\psi K_s^0(\pi\pi)$ (right). For all observed B-hadrons the measured masses are in good agreement with the PDG values.

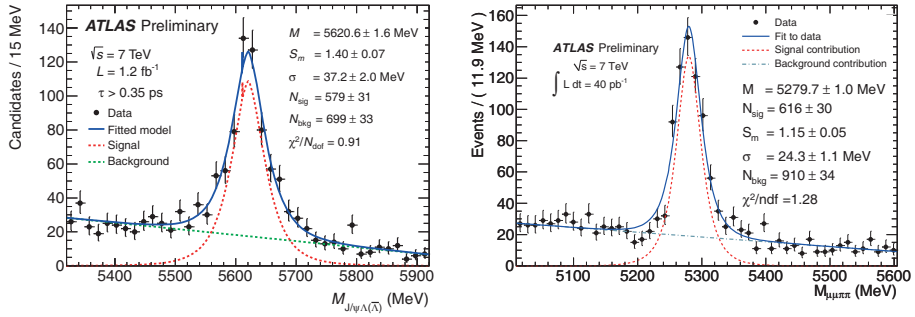

Fig. 6. – Left: Distribution of the invariant mass of $\Lambda_b \to J/\psi\Lambda(p^+\pi^-)$ and right: $B_d \to J/\psi K_s^0(\pi\pi)$ candidates reconstructed in data after a proper decay time cut of 0.35 ps.

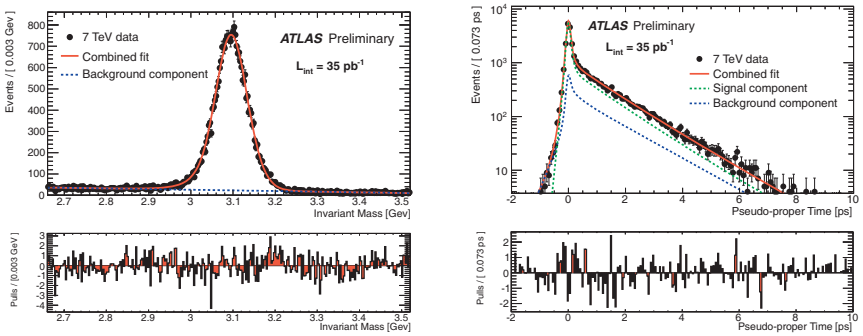

Fig. 7. – Invariant mass (left) and pseudo-proper time (right) projections (with respective pull distributions) of the simultaneous fit to these distributions in the average B-hadron lifetime measurement.

Precise measurement of B-hadron lifetimes allow tests of theoretical predictions. Lifetime ratios for different species of B-hadrons are predicted by theory at the per cent level. The lifetime difference of the two mass eigenstates of the B_s^0 system allows the measurement of the B_s^0 mixing phase which generates CP violation in the $B_s^0 \to J/\psi\phi$ channel.

Before making such measurements the performance of the track and secondary vertex reconstruction can be validated by measuring the lifetime of inclusive $B \to J/\psi(\mu^+\mu^-)X$ decays. This inclusive sample has orders of magnitude higher statistics that fully reconstructed exclusive B-hadrons. The average B-lifetime is extracted from the data by peforming an unbinned maximum-likelihood fit simultaneously to the J/ψ invariant mass and pseudo-proper decay time [8]. A correction factor is applied for the smearing introduced by the use of the pseudo-proper time to extract the real B-hadron lifetime. This factor is obtained from MC where the J/ψ momentum spectrum is re-weighted to match the BaBar data. Figure 7 shows the invariant mass and pseudo-proper time projections

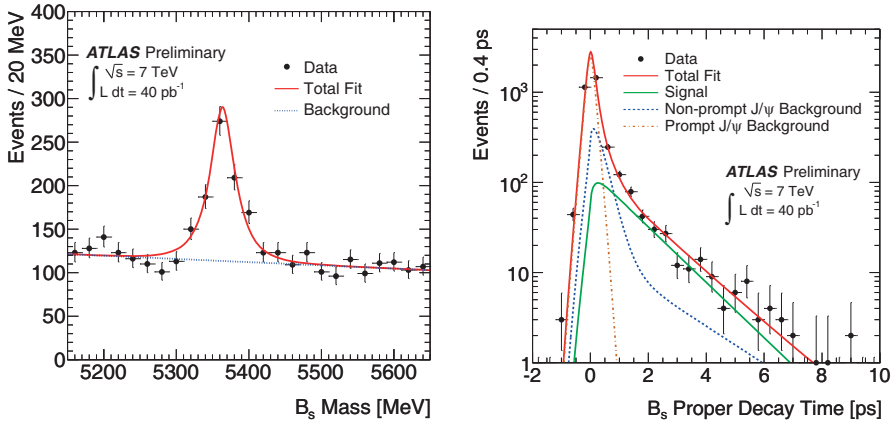

Fig. 8. – Invariant mass (left) and B_s^0 proper decay time (right) of reconstructed $B_s^0 \to J/\psi\phi$ decay candidates. The points with error bars are data. The solid line is the mass projection of the simultaneous mass and lifetime fit. Also shown are the fitted signal, prompt and non-prompt background distributions.

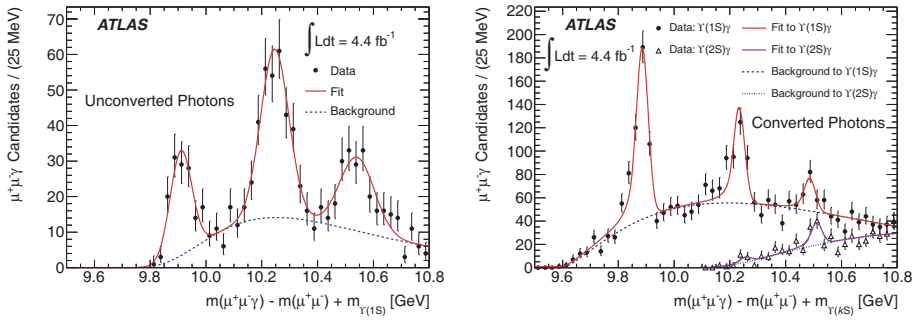

Fig. 9. – The mass distribution of $\chi_b \to \Upsilon(kS)\gamma$ $(k = 1, 2)$candidates for unconverted photons (left) and converted phtons (right). The data for decays of $\chi_b \to \Upsilon(1S)\gamma$ and $\chi_b \to \Upsilon(2S)\gamma$ are plotted using circles and triangles, respectively. Solid lines represent the total fit result for each mass window. The dashed lines represent the background components only.

from the fit. The measured average B-hadron lifetime is $1.1489 \pm 0.016 \pm 0.043$ ps. The main systematic uncertainty in this measurement is from the uncertainty in the radial alignment of the Inner Detector. The result is in agreement with the expected average lifetime computed using PDG lifetimes and production fractions from the different B-hadron species. Lifetimes of the B_d^0 and B_s^0 mesons are measured using the exclusive decay modes $B_d^0 \to J/\psi K^*$ and $B_s^0 \to J/\psi\phi$ [9]. Since in this case the B-hadron is fully reconstructed the proper decay time ($\tau = L_{xy} m^B / p_T^B$) can be used together with the mass in order to extract the yield, mass and lifetime in each channel. Figure 8 shows the mass and proper time disributions for the $B_s^0 \to J/\psi\phi$ candidates. These measurements use the full 2010 dataset and yield 2750 B_d^0 and 463 B_s^0 signal events. The lifetimes are measured to be

$$\tau_{B_d^0} = 1.51 \pm 0.04(\text{stat.}) \pm 0.04(\text{syst.})\,\text{ps}, \tag{2}$$

$$\tau_{B_s^0} = 1.41 \pm 0.08(\text{stat.}) \pm 0.05(\text{syst.})\,\text{ps}. \tag{3}$$

4. – Observation of $\chi_b(3P)$

The P-wave $b\bar{b}$ χ_b states can be reconstructed in ATLAS through the radiative decay to Υ. The $\chi_b(1P)$ and $\chi_b(2P)$ states have already been observed through this decay mode at other experiments. Using $4.4\,\text{fb}^{-1}$ of data from 2011, ATLAS has made the first observation of the $\chi_b(3P)$ state [10].

Pairs of oppositely charged muons are fit to a common vertex and required to have an invariant mass in the ranges $9.25 < m_{\mu\mu} < 9.65\,\text{GeV}$ and $9.80 < m_{\mu\mu} < 10.10\,\text{GeV}$ in order to select $\Upsilon(1S)$ and $\Upsilon(2S)$ candidates. Photons are reconstructed either directly in the calorimeter or through a conversion to e^+e^-. χ_b candidates are formed by combining a reconstructed $\Upsilon \to \mu^+\mu^-$ candidate with a reconstructed photon candidate. The invariant mass difference $\Delta m = m(\mu\mu\gamma) - m(\mu\mu)$ is calculated in order to minimise the effect of $\Upsilon \to \mu\mu$ mass resolution. In order to compare the Δm distributions for the $\Upsilon(1S)\gamma$ and the $\Upsilon(2S)\gamma$ the variable $\tilde{m}_k = \Delta m + m_{\Upsilon(kS)}$ is defined, where $m_{\Upsilon(kS)}$ are the world average masses [11] of the $\Upsilon(kS)$ states.

Figure 9 shows the distribution for unconverted photons (left) and converted photons (right). In addition to the expected peaks for $\chi_b(1P, 2P) \to \Upsilon(1S, 2S)\gamma$, structures are observed at an invariant mass of approximately 10.5 GeV. These additional structures are interpreted as the radiative decays of the previously unobserved $\chi_b(3P)$ states, $\chi_b(3P) \to \Upsilon(1S)\,\gamma$ and $\chi_b(3P) \to \Upsilon(2S)\,\gamma$. The higher threshold for unconverted photons (2.5 GeV *versus* 1 GeV for converted photons) prevents the reconstruction of the soft photons from $\chi_b(2P, 3P)$ decays into $\Upsilon(2S)$. An unbinned maximum likelihood fit is performed to the $\tilde{m_k}$ distributions, the mass for $\chi_b(3P)$ is found to be consistent in the unconverted and converted photon cases. Since the uncertainty on the conversion measurement is smaller this is used for the final mass determination of $10.539 \pm 0.005(\text{stat.}) \pm 0.009(\text{syst.})$ GeV.

5. – Summary and outlook

The ATLAS B-physics programme has made many interesting and important measurements of production cross-sections which are already providing important input for theoretical models. ATLAS has also observed many B-hadrons and made measurements of masses and lifetimes. These measurements are in agreement with PDG values and demonstrate the experimental techniques which will be needed for future measurements including searches for CP violation and rare B decays. The first observation of the $\chi_b(3P)$ state is reported. New results on CP violation measurements and rare decay searches using the 2011 dataset can be expected soon.

REFERENCES

[1] ATLAS Collaboration, *JINST*, **3** (2008) S08003.
[2] ATLAS Collaboration, *Nucl. Phys. B*, **850** (2011) 387.
[3] Cacciari M. *et al.*, *JHEP*, **05** (1998) 007; *JHEP*, **03** (2001) 006.
[4] Lansberg J. P., *Eur. Phys. J. C*, **61** (2009) 693.
[5] Ullrich t. *et al.*, *Phys. Rep.*, **462** (2008) 125.
[6] ATLAS Collaboration, *Phys. Lett. B*, **705** (2011) 9.
[7] ATLAS Collaboration, ATLAS-CONF-2010-098, ATLAS-CONF-2011-050, ATLAS-CONF-2011-105, ATLAS-CONF-2011-124, ATLAS-CONF-2011-136.
[8] ATLAS Collaboration, ATLAS-CONF-2011-145.
[9] ATLAS Collaboration, ATLAS-CONF-2011-092.
[10] ATLAS Collaboration, *Phys. Rev. Lett.*, **108** (2012) 152001.
[11] Nakamura K. *et al.* (Particle Data Group), *J. Phys. G*, **37** (2010) 075021.